Article

A click-type protein-DNA conjugation for Mn imaging in living cells

Shanfang Hu, Jinghui Zhang, Rui Tang, Jiahui Fan, Huiqiong Liu, Wenyuan Kang, Chunyang Lei, Zhou Nie, Yan Huang, and Shouzhuo Yao

Anal. Chem., **Just Accepted Manuscript** • DOI: 10.1021/acs.analchem.9b02191 • Publication Date (Web): 04 Jul 2019

A click-type protein-DNA conjugation for Mn^{2+} imaging in living cells

Shanfang Hu[1], Jinghui Zhang[1], Rui Tang, Jiahui Fan, Huiqiong Liu, Wenyuan Kang, Chunyang Lei, Zhou Nie*, Yan Huang*, Shouzhuo Yao

State Key Laboratory of Chemo/Biosensing and Chemometrics, College of Chemistry and Chemical Engineering, Hunan Provincial Key Laboratory of Biomacromolecular Chemical Biology, Hunan University, Changsha 410082, P. R. China.

ABSTRACT: A click-type protein-DNA conjugation, named as MnDDC (Mn^{2+}-activated DCV-DNA conjunction), is presented, where DCV (rep protein of duck circovirus) and its target DNA work as the modular blocks to rapidly and effectively generate Mn^{2+}-dependent and site-specific protein-DNA linkage. On the basis of MnDCC, a fluorescent Mn^{2+} biosensor composed of DCV and a molecular beacon, was developed for rapid sensing of Mn^{2+} within 2 min with nanomolar sensitivity. Using the proposed biosensor, not only analysis of Mn^{2+} in real samples (e.g. serum and food), but also wash-free fluorescent imaging of Mn^{2+} in extracellular environment and cytoplasm have been achieved. Moreover, the MnDDC-based sensor was proved to be a powerful tool for visualization of Mn^{2+} during exploration of the associated cytotoxicity in living neural cells, which is helpful to reveal the cellular responses towards the disordered homeostasis of Mn^{2+} in both extracellular and intracellular microenvironments.

Click chemistry is a class of reactions for joining small modular units together, with very high yields, minimal and inoffensive byproducts under simple reaction conditions.[1] Due to its high efficiency and selectivity, and modular blocks, click chemistry has found broad applications in pharmaceutical science, materials chemistry and biological chemistry since the concept was first introduced in 2001.[1-3] Moreover, its unique qualities, such as one-pot reaction in a benign solvent (such as water), as well as quick and irreversible yield of a single reaction product with high reaction specificity, make it particularly suitable to be used in complex biological environments.[1, 2] Recently, various molecules in live cells were incorporated with click modular units for pulldown experiments, super-resolution imaging,[4] and protein/nucleotide modification,[5, 6] where the classic click reaction, the copper-catalyzed azide-alkyne cycloaddition (CuAAC), was widely applied.[7-9] While the click reactions with new modular blocks are still highly desired, especially for the site-specific conjugation between biomacromolecules.

Protein-DNA conjugation has aroused growing interest for academia and industry applications, as it combines the diverse functionalities of proteins with the precise recognition and encoding abilities of DNA.[10, 11] For different utilities, site-specific covalent protein-DNA linkage is almost always highly needed.[12] Many chemical and genetic methods have been developed for targeted conjugation between protein and DNA,[10-14] but strategies with high reaction rate, specificity and biocompatibility, are still limited.[10, 11] Click chemistry seems an ideal way to solve the problems, while was largely ignored. Very recently, a robust method for site-specific and covalent linkage of proteins and DNA was reported, where HUH endonuclease domains were designed as the modular units to link with synthetic oligonucleotides that contain the ori sequences of endonucleases.[15-17] DCV, a truncated replication initiation protein (Rep, 1-120 aa) of duck circovirus, is a member of the HUH endonuclease superfamily.[18] Here, we found that the metal ion-activated DCV-DNA conjugation can perform in aqueous environment with high efficiency, and is robust under fluctuating

conditions (temperature, pH and buffer). Moreover, DCV showed excellent selectivity towards Mn^{2+} over other divalent metal ions, such as Ca^{2+} and Mg^{2+}. Hence, using DCV and its target oligonucleotide as the modular blocks, the Mn^{2+}-activated DCV-DNA conjugation (MnDDC) is characterized as a click-type reaction. Analogous to CuAAC (Scheme 1A), the efficient and covalent linkage of the two modular units in MnDDC is activated by a metal ion.

Manganese is an essential element for human health, since Mn^{2+} function as cofactors for a large variety of functional proteins, including enzymes (oxidoreductases, transferases, hydrolases, lyases, isomerases, ligases, etc.) and other Mn^{2+}-binding proteins (transcription factors, lectins, and integrins, etc.).[19-21] Excessive exposure of Mn^{2+} poses a potential threat to cells and may lead to serious diseases, such as neurodegenerative disorder and childhood developmental disorders.[21, 22] The important role and wide distribution of Mn^{2+} in biological system, as well as its extensive utility as an excellent MRI contrast agent, have attract much attention to develop methods for Mn^{2+} probing in biological and environmental samples.[23] However, the development of fluorescent Mn^{2+} sensors has been challenged by its chemical similarity with Mg^{2+}/Ca^{2+} and the fluorescence quenching originated from the paramagnetic nature of Mn^{2+}.[23] To address these problems, the click-type MnDDC reaction was deployed as a fluorescent sensor for Mn^{2+} assay, where a molecular beacon was utilized for DCV-DNA ligation and signal readout (Scheme 1B). The intrinsic clickable characteristics enable the sensor to realize selective analysis of Mn^{2+} not only in serum and food samples, but also on cell surface and in cytoplasm (Scheme 1C). Moreover, taking human neuroblastoma cell line SHSY5Y as an *in vitro* model of dopaminergic neurons, Mn^{2+} imaging during exploration of the associated oxygen species (ROS) generation, and the concentration-dependent relationship between Mn^{2+} and its known neuropathological consequence, tyrosine hydroxylase (TH) down regulation (Scheme 1C), have been verified with the use of the MnDDC-based biosensor.

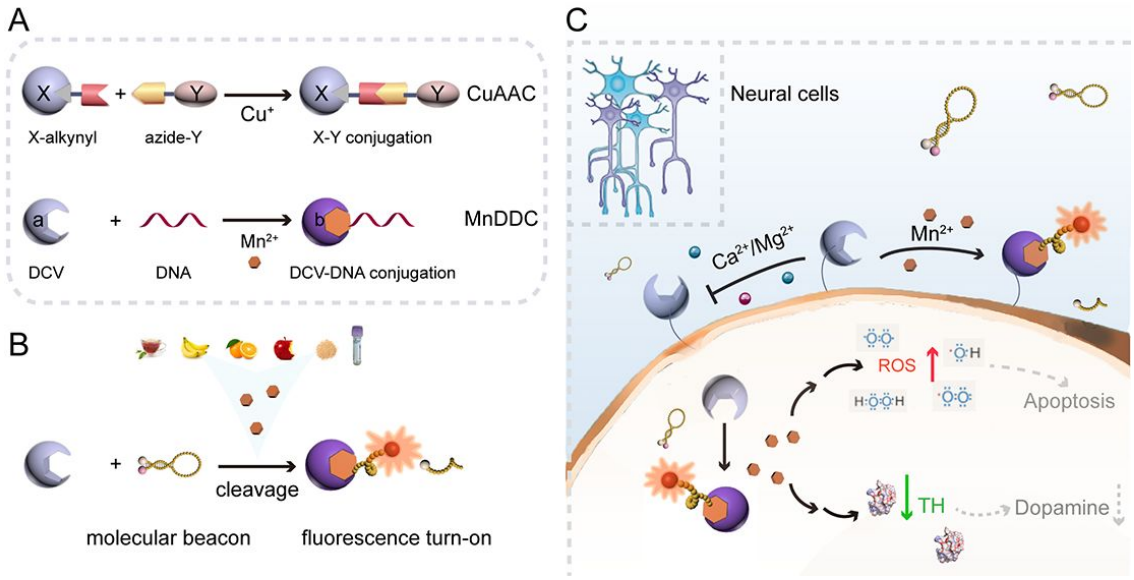

Scheme 1. Schematic illustration of MnDDC and its applications for Mn^{2+} sensing. (A) Analogy between MnDDC and CuAAC. (B) Fluorescent "turn on" assay of Mn^{2+} in real samples based on MnDDC. (C) Mn^{2+} imaging in cytosol and on cell surface in neural cells, and the cellular responses towards the disordered homeostasis of Mn^{2+}.

EXPERIMENTAL SECTION

Construction, Expression and Purification of DCV. Sequence of DCV was referred to the reported literature.[17] DCV gene was inserted into pET-28a with the restriction enzyme cutting sites of *BamH*I/*Hind*III, and plasmid pET 28a-*dcv* was constructed by Sangon (Shanghai, China).

The reconstructed plasmid was transformed into *E. coli* BL21 (DE3) by heat shock. Cells were grown in LB medium at 37 °C until OD_{600} (optical density at 600 nm) reached about 0.6, and then were induced with 0.6 mM isopropyl β-D-1-thiogalactopyranoside (IPTG) at 15 °C for 24 h. Cells were harvested by centrifugation and re-suspended in binding buffer (10 mM Tris, 2 M NaCl, pH 7.4), and then lysed by sonication. Protein was purified by Ni-NTA agarose chromatography (ÄKTA, GE), and then the buffer was exchanged into desalination buffer (10 mM Tris, 100 mM NaCl, 50% glycerin, pH 7.4) by desalination chromatography (ÄKTA, GE). The purified DCV was quantified by BCA protein determination reagent and stored at -80 ℃.

SDS-PAGE Analysis of MnDDC. For SDS-PAGE, the reactions were performed in HEPES buffer (50 mM HEPES, pH 8.0, 150 mM NaCl, and 1 mM $MnCl_2$) and incubated at 20 ℃ for 15 min, and then stopped with 5X loading buffer. The reactions were analyzed by gel-shift assay on 12% denaturing polyacrylamide gels (Bio-Rad Stain-Free gels). Theoretical molecular weight of DCV was evaluated on the net (http://web.expasy.org/compute_pi/).

Turn on Fluorescence Assays. Molecular beacon (MB) was synthesized with a quencher (BHQ2) and TAMRA at their 5' and 3' terminals, respectively, and dissolved at 100 μM in 150 mM NaCl. Unless otherwise noted, MnDDC were performed in HEPES buffer (50 mM HEPES, pH 8.0, 150 mM NaCl, and 1 mM $MnCl_2$) and incubated at 20 ℃ for 2 min before testing. Fluorescence of TAMRA was measured on a Quanta Master TM4 fluorescence spectrophotometer (PTI, Canada).

Detection of Mn^{2+} in Food Samples. The samples were weighed and crushed. Then the samples were fired in muffle for 12 h at 550 ℃. After that, samples were added with 5 mL HNO_3 (1%) and dissolve overnight on electric hot plate. After evaporation of HNO_3, the samples were diluted with H_2O to volume of 25 mL. Then 50 μL supernatant was added to 50 μL MnDDC solution, and after incubated in 20 ℃ for 2 min, fluorescence was measured.

Cell Culture. Cells were cultured in DMEM medium at 37 ℃ with 5% CO_2. DMEM medium was supplemented with 10% fetal bovine serum (FBS), 1% L-glutamine and 1% antibiotic-antimycotic (100 units/mL of penicillin, 100 μg/mL of streptomycin, and 0.25 μg/mL of Amphotericin B). Cell numbers were measured with a TC10 automated cell counter (Bio-Rad, USA).

Fluorescence Imaging of Mn^{2+} Assay inside Cells. Cells (2×10^4 cells/well) were seeded in a confocal dish (Cellvis, USA). After cultured for 24 h, cells were transfected with molecular beacon (MB) (100 nM) and DCV (1 μM) using Lipofectamine 3000 (Thermo Fisher) at 37 °C. After 12 h, cells were washed and the culture medium was replaced with PBS supplemented with 0.5 mM Mn^{2+}. Cells were cultured at 20 °C for 0.5 h. After incubation, cells were washed three times with PBS. Imaging was performed with a confocal laser scanning microscope (CLSM, Nikon A1 plus, Japan) using a 60×objective. Hoechst 33342 and TAMRA were visualized with 405 and 561 nm excitation laser, respectively.

Surface Display of GFP-DCV in Mammalian Cells. Sequence of GFP was referred to the reported literature.[24] Genes encoding GFP-DCV was inserted into pDisplay with the restriction enzyme cutting sites of *Bgl*II/*Pst*I, which introduces a C-terminal platelet-derived growth factor receptor (PDGFR) transmembrane domain. The construct pDisplay-*gfp-dcv* was transfected into mammalian cells using Lipofectamine 3000 (Thermo Fisher). After 48 h incubation, GFP-DCV was displayed on cell surface, then fluorescence imaging was performed on a confocal laser scanning microscope.

Fluorescence Imaging of Mn^{2+} on Cell Surface. Cells (2×10^4 cells/well) were seeded in a confocal dish (Cellvis, USA), and cultured in DMEM at 37 °C for 24 h. The cells were transfected with pDisplay-*gfp-dcv* or pDisplay-*dcv* using Lipofectamine 3000 (Thermo Fisher) and incubated for 48 h. Then the culture medium was replaced with DMEM containing 100 nM molecular beacon (MB) and 0.5 mM Mn^{2+}. After being cultured at 20 °C for 0-5 min, imaging was performed with a confocal laser scanning microscope (CLSM, Nikon A1 plus, Japan) using a 60×objective. Hoechst 33342, GFP and TAMRA were visualized with 405, 488 and 561 nm excitation laser, respectively. The fluorescence intensity distributions of each pixel and the semi-quantitative fluorescence intensity were determined by Python and Image J software, respectively.

Cytotoxicity Assay in Vitro. The cytotoxicity of different reagents was determined by CCK8 assay. Briefly, cells (2×10^4 cells/well) were seeded on a 96-well plate and incubated for 24 h. The medium was replaced with 200 μL full medium containing the indicated compound and further incubated in 37 °C for several hours. Afterward, CCK8 (20 μL per well) was added. Three hours later, the optical density at 450 nm (OD_{450}) was determined via a microplate reader. Cell viability was calculated based on the formula: Cell viability $= [(OD_{sample} - OD_{buffer})/(OD_{cell} - OD_{buffer})] * 100\%$. OD_{sample}, OD_{cell} and OD_{buffer} are the OD_{450} value of the cells treated with sample, cells without any treatment, and the culture medium supplemented with CCK8, respectively.

Simultaneous Imaging of Mn^{2+} and Reactive Oxygen Species (ROS) in SHSY5Y cells. Mn^{2+} was detected by MnDDC assay. Generation of ROS was assessed by an oxidation-sensitive fluorescent probe DCFH-DA (2′,7′-Dichlorofluorescin diacetate) in ROS assay kit. DCFH-DA is a nonpolar compound that readily defuses into cells, where it is de-esterified intracellularly and turns to highly fluorescent DCF (2′,7′-dichlorofluorescein) upon oxidation by ROS.

Briefly, SHSY5Y cells (2×10^4 cells/well) were seeded in a confocal dish (Cellvis, USA) and cultured for 24 h. The cells were transfected with DCV (1 μM) using Lipofectamine 3000 (Thermo Fisher) and incubated with Mn^{2+} (500 μM) at 37 °C for 12 h. Then the cells were washed three times with PBS and transfected with molecular beacon (MB, 100 nM) for 2 h. After treatment, cells were washed with PBS and loaded with 10 μM DCFH-DA in serum free DMEM at 37 ℃ for 20 min. The cells were again washed three times with serum free DMEM. Imaging was performed with a confocal laser scanning microscope (CLSM, Nikon A1 plus, Japan) using a 60×objective. ROS signal (the DCF fluorescence) was observed with a 488 nm laser (green channel) and Mn^{2+} signal (TAMRA fluorescence in MnDDC assay) was observed with a 561 nm laser (red channel).

Preparation of the Cell Lysates and Western Blotting. The SHSY5Y or U251 cells were seeded in six-well culture dishes and cultured in DMEM for 24 h. Subsequently, the cells were cultured in DMEM containing Mn^{2+} (0-250 μM) for 12 h at 37 °C. Then the dishes were put on ice and washed twice by precooling PBS, and the cells were lysed with lysis buffer (RIPA buffer with 1% phosphatase inhibitors and protease inhibitor) for 10 min. The cell lysates were collected and centrifuged in 4 ℃ with 14000 rpm for 10 min. The supernatant was stored at -20 ℃ before use.

The cell lysates were separated by 8% SDS-PAGE electrophoresis, and transferred to nitrocellulose membrane by semi-dry electrophoretic transfer unit for 12 min. After blocking with 5% skim milk-PBST (1× PBS with 0.1% Tween-20) solution for 1 h, the membrane reacted with primary antibody (1:500 dilution) overnight in 4 ℃. After washing three times with PBST, the membrane was incubated with secondary antibody (goat anti-mouse IRdye 680RD, 1:10000 dilution) for 1 h at room temperature. Images were obtained using near-infrared imaging system (LICOR, USA).

Immunofluorescence Analysis. SHSY5Y cells (2×10^4 cells/well) were seeded in a confocal dish (Cellvis, USA) and cultured for 24 h. Being treated with Mn^{2+} (0-250 μM) at 37 ℃ for 12 h, the cells were fixed with

4% paraformaldehyde at 25 °C for 15 min, washed three times with PBS, permeabilized with 0.4% Triton X-100 in PBS at 25 °C for 12 min, washed three times with PBS, and blocked with 10% goat serum in PBS for 1 h. The fixed and permeabilized cells were incubated with primary antibody (TH antibody, 1:100 diluted) overnight at 4 ℃, washed three times with PBS, and incubated with Anti-Mouse IgG (whole molecule)-FITC antibody (1:200 delution) at 25 ℃ for 2 h sequentially. Nuclei were visualized by 4,6-diamidino-2-phenylindole staining (DAPI, 0.02 μg/ml). After washing three times with PBS, cells were imaged on a confocal laser scanning microscope (CLSM, Nikon A1 plus, Japan) using a 60×objective. DAPI and TH signal (FITC) were visualized with 405 and 488 nm excitation laser, respectively.

RESULTS AND DISCUSSION

Characterization of the Mn^{2+}-Activated DCV-DNA Conjugation (MnDDC) Reaction. For quantitative analysis of the MnDDC reaction, a molecular beacon (MB) with the specific recognition sequence of DCV (AAGTATT^ACCAG, Table S1)[17] in the loop was used as the DNA module, where the 3' and 5' ends were labeled with a fluorophore (TAMRA) and a quencher (BHQ2), respectively (Table S1). In the presence of proper divalent metal ions, DCV is activated and cleaves the T^A phosphodiester bond in the loop, and then covalently links to the 5′-phosphate of the ACCAG containing segment, leading to the formation a DCV-DNA conjugation.[17] Meanwhile, the quencher and the fluorophore are separated, which results in the fluorescence readout (Scheme 1B). Therefore, the divalent metal ion-activated DCV-DNA ligation can be monitored by the fluorescence enhancement.

Based on the design, the MnDDC reaction was firstly analyzed by gel shift assay. Since physiological cofactor of DCV was unknown, Mn^{2+}, one of the physiological cofactors of other HUH endonuclease superfamily membranes,[25] was tested. DCV, Mn^{2+}, and hairpin were simply mixed in HEPES buffer and incubated at 20 ℃. In the presence of Mn^{2+} and excess MB, the band of DCV was almost dismissed along with the appearance of a retardation band of DCV-DNA conjugation (Figure 1A, lane 2). Semi-quantitative result quantified by ImageJ revealed that 90% of DCV was converted into DCV-DNA conjugation. While in the absence of Mn^{2+} or in the presence of Mn^{2+} and metal ion chelator (EDTA), no obvious band of the conjugation was observed (Figure 1A, lanes 3-4). Moreover, the similar results of the fluorescent experiments (Figure 1B) also demonstrated the crucial role of Mn^{2+} in the MnDDC reaction. Kinetic curve monitored by the real-time fluorescence changes at 580 nm indicated that the reaction was very rapid and reached equilibrium in 2 min (Figure 1C), which is of great value for fast detection and imaging. In addition, the reaction kept high ligation efficiencies (>90%, determined based on DCV) in various reaction buffers (pH 6.0-8.0, Figure S1 and S2) at temperature range from 20 ℃ to 42 ℃, and even maintained a high ligation efficiency of 60% at 4 ℃ (Figure S3). Finally, the effects of other metal ions on the MnDDC reaction were investigated. Although Ca^{2+} and Mg^{2+} show high similarity in structural and electronic symmetry with Mn^{2+}, they cannot induce obvious fluorescence response even at a high concentration of 100 μM. Besides, neither the abundant metal ions in biological fluids, such as Zn^{2+}, Fe^{3+}, and K^{+} (Table S2),[26] nor the other common divalent and trivalent ions caused obvious fluorescence change (Figure 1D). Although other HUH endonuclease superfamily membranes use various divalent metal ions as cofactors in vitro,[15, 25] we have demonstrated that DCV is highly specific to Mn^{2+} over Ca^{2+}, Mg^{2+} and other common metal ions. Taken together, MnDDC was characterized as rapid reaction with high efficiency, good selectivity in moderate and fluctuant environment. Quite similar to CuAAC, MnDDC in principle meets the criteria of click reaction.[1, 2, 27, 28] It is worthy to note that the protein nature of DCV makes it facile to be fused with other functional proteins or peptides, enabling it to serve as a modular block in site-specific protein-DNA conjugation. Furthermore, taking advantage of the high specificity of MnDDC, we sought to explore its potential in the development of new analytical approaches for Mn^{2+} sensing.

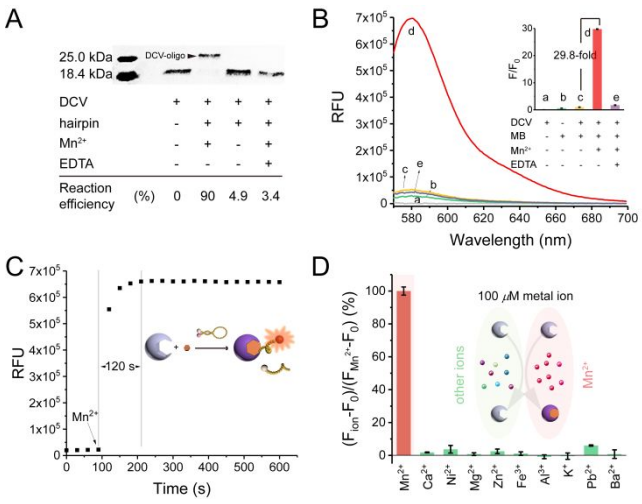

Figure 1. Characterization of the Mn^{2+}-activated DCV-DNA conjugation (MnDDC). Analysis of MnDDC by (A) SDS-PAGE and (B) fluorescence spectra using MB. The mixture was incubated in HEPES buffer (pH 8.0) at 20 ℃ for 15 min. [DCV] = 4 μM, [hairpin] = 10 μM, [MB] = 100 nM, [Mn^{2+}] = 1 mM, [EDTA] = 1 mM. F and F_0 are the fluorescence intensities of the tested sample and the metal ion free control (DCV + MB) at 580 nm, respectively. (C) Time scanning of the fluorescence intensity change of MnDDC. [DCV] = 4 μM, [MB] = 100 nM, [Mn^{2+}] = 1 mM. The mixture was incubated in HEPES buffer (pH 8.0) at 20 ℃ for 2 min. (D) Specificity of MnDDC based on the relative fluorescence intensity. F_{Mn2+} and F_{ion} are the fluorescence intensities of Mn^{2+} and other metal ion added samples at 580 nm, respectively. [DCV] = 4 μM, [MB] = 100 nM, [metal ions] = 100 μM. The mixture was incubated in HEPES buffer (pH 8.0) at 20 ℃ for 2 min.

In Vitro Assay of Mn^{2+} Based on MnDDC. To obtain the optimal sensing performance for Mn^{2+}, several parameters were investigated based on the fluorescence response of the MnDDC reaction. Considering that the stem length and the temperature greatly affect the structure stability of MB, the influences of them on the assay of Mn^{2+} were analyzed firstly. As shown in Figure S4 and S5, 29.8 fold fluorescence response was obtained using MB1 with a 5-nucleotide stem at 20 ℃, while the response decreased sharply to 3.5-fold when the stem was changed to 6-nucleotide (molecular beacon 2), and the increase of the reaction temperature to 37 ℃ also significantly decreased the fluorescence to 13.4-fold. Since the fluorescence signal was generated by the Mn^{2+}-mediated cleavage of MB by DCV, the concentration of DCV was optimized under a fixed concentration of MB (100 nM). As revealed in Figure S6, the fluorescence signal was positively related to the concentration of DCV, and reached saturation at 4.0 μM. Further, Figure S7 showed that fluorescence enhancements triggered by Mn^{2+} were reproducible in the range of pH 6-9, indicating that the MnDDC-based assay is available in samples with fluctuant acidity. Hence, Mn^{2+} measurement was carried out with 4 μM DCV, 100 nM MB (MB1), and incubated at 20 ℃ for 2 min in HEPES buffer (pH 8.0).

Under the optimized conditions, different concentrations of Mn^{2+} were tested by the MnDDC-based assay. The fluorescence intensity increased gradually with the addition of 0-800 μM Mn^{2+} (Figure 2A). Accordingly, the obtained fitting curve exhibited two linear ranges, with the concentration range from 0.05 to 8 μM and 8 to 800 μM, respectively (Figure 2B). The detection limit reaches nanomolar level (50 nM) for free Mn^{2+} ions, which is far lower than the US Environmental Protection Agency standard for Mn^{2+} in drinking water (5 μM) and the Mn^{2+} concentration in some pathological tissues (micromolar).[21, 22, 29, 30] Additionally, compared with several existing Mn^{2+} detection methods, such as organic probe-based and nanomaterial-based methods, the intrinsic clickable characteristics enable the MnDDC-based assay showed merits with better selectivity, broader response range, and lower limit of detection (Table S3).[31, 32]

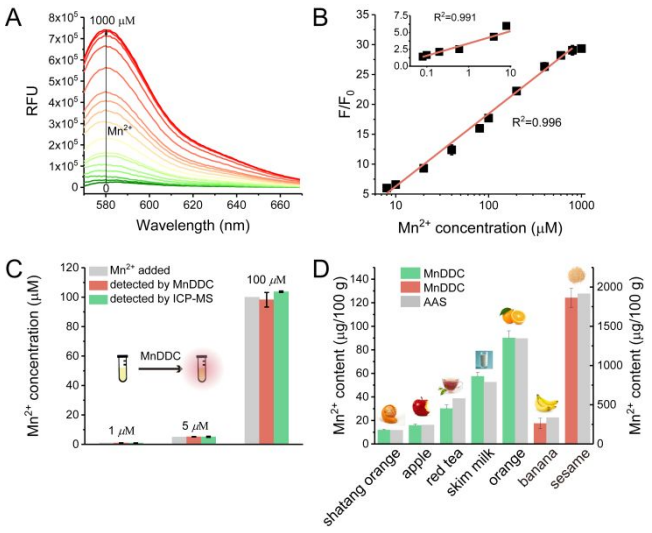

Figure 2. (A) Fluorescence response of the MnDDC-based assay to different concentrations of Mn^{2+}. (B) The linear correlation between the relative fluorescence intensity and the concentration of Mn^{2+} in the ranges of 0.05-8 μM and 8-800 μM, respectively. F and F_0 are the fluorescence intensities of the tested sample and the Mn^{2+} free control (DCV + MB) at 580 nm, respectively. (C) Detection of Mn^{2+} in 10% serum samples. (D) Determination of Mn^{2+} content in different food samples. [DCV] = 4 μM, [MB] = 100 nM.

Serum Mn^{2+} level is usually used as a crucial marker for diagnosis of related diseases, such as Parkinson's disease and manganism.[21] Serum Mn^{2+} level in health human body is in the range of 7-15 nM, and increases to micromole level in some pathological serum samples.[26, 33] However, the physiological concentration of Ca^{2+}, Mg^{2+} in serum are also at millimole level (Table S2), and the influence of them is a challenge for the specific Mn^{2+} sensing in serum.[23, 26] Here, the feasibility of the MnDDC-based assay for Mn^{2+} detection in serum sample was investigated. A standard addition method was used to prepare samples that are comparable to pathological serum samples. The concentrations of Mn^{2+} in these samples were detected by our assay and the standard inductively coupled plasma mass spectrometry (ICP-MS), respectively. The recovery of this method varied from 94.8% to 104.5%, and the RSDs ranged from 2.89% to 4.99% (Table S4), demonstrating that the assay provided an accurate measure of serum Mn^{2+}.

Daily Mn intake is an important index for human health.[21] The Institute of Medicine's Dietary Reference Intake for Mn cites approximately 2000 μg/day as adequate intake for adults, and 1200–1500 μg/day for children.[21] Daily requirements of Mn^{2+} are commonly met by the adequate diet.[21, 30] Hence, the detection of Mn^{2+} in the numerous dietary sources is of great significance to give a dietary guide. Here, Mn^{2+} in various dietary sources including fruits and milk, were extracted by ashing method and analyzed by the MnDDC-based assay. A wide Mn^{2+} content range (11.8-1863 μg/100 g) was observed from these food samples, which was in accordance with the data obtained by atomic absorption spectroscopy (AAS, Figure 2D), indicating the practicability of the MnDDC-based assay in samples with different abundance of Mn^{2+}.

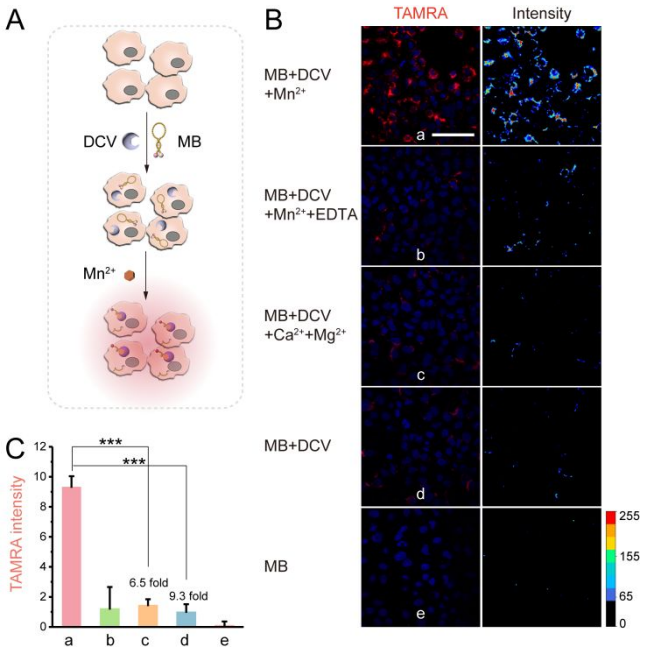

Figure 3. (A) Schematic of the fluorescence imaging of Mn^{2+} inside A549 cell. (B) Intracellular fluorescence imaging (left) and the corresponding color-coded (right) TAMRA signal from MnDDC inside A549 cell. Red: TAMRA, blue: Hoechst 33342. Scale bar is 100 μm. (C) Semi-quantitative analysis of TAMRA intensity in Figure 3B. Cells were transfected with DCV and MB by Lipofectamine 3000 for 12 h, and then were washed and further incubated with Metal ions for another 0.5 h before detection. [DCV] = 1 μM, [MB] = 100 nM, [Mn^{2+}] = 500 μM, [Mg^{2+}] = 250 μM, [Ca^{2+}] = 250 μM, [EDTA] = 500 μM. Data points represent mean ± SD (n = 10). ***$p < 0.001$.

Mn^{2+} Monitoring in Living Cells. Intracellular Mn^{2+} is an indispensable cofactor for various vital biological processes, including redox equilibrium maintenance in mitochondria, deoxyribonucleotides formation and enzymatic transformations.[21, 23, 26] Tracing intracellular Mn^{2+} level can improve our understanding of intracellular Mn^{2+} trafficking and the regulation of Mn homeostasis. The robust performance of the MnDDC-based assay in aqueous solution suggested that it might be capable for probing the intracellular uptake of Mn^{2+}. Here, the feasibility of the sensor for Mn^{2+} imaging in living cells was tested using the non-small cell lung cancer cells (A549) as a model (Figure 3). The two components of the MnDDC-based sensor, DCV and MB, were transfected into A549 cells by Lipofectamine 3000. After incubation of the cells with exogenously added Mn^{2+}, bright red fluorescence signals were detected in the cytoplasm of the A549 cells (Figure 3B), indicating the occurrence of MnDDC and the cleavage of MB, accompanied by the drastic increase of the red fluorescence. Conversely, negligible red fluorescence signals were observed in the control groups. Moreover, the semi-quantitative results showed that the red fluorescence signal in the cells treated with Mn^{2+} was approximately 9.3-fold and 6.5-fold to that without Mn^{2+} or with Ca^{2+} and Mg^{2+}, respectively (Figure 3C). These results revealed that the MnDDC-based sensor provides a useful tool for specific imaging of Mn^{2+} in living cells.

Wash-Free Imaging of Extracellular Mn^{2+}. Extracellular Mn^{2+} plays a critical role in physiological signal pathways.[21] Imaging of Mn^{2+} fluctuations in extracellular microenvironment can substantially extend our insight into Mn^{2+}-mediated cellular responses and cell-to-cell interactions. Although several probes realized Mn^{2+} tracing in living cells (Table S3), the lacking of subcellular localization module hindered their application for sensing of extracellular Mn^{2+}. The protein nature of DCV makes it be easily fused with subcellular targeting blocks, thus providing a potential general strategy for subcellular localization and sensing. Herein, we

transfected human leukemic cells (CEM) with pDisplay-*egfp-dcv* for analysis of dynamic Mn^{2+} fluctuation on mammalian cell surface. pDisplay is a mammalian expression vector[34] that enables display of DCV and EGFP on the extracellular membrane. The bright green fluorescence on the periphery of the cells (Figure 4) indicated the successful expression of EGFP-DCV on the extracellular side of the plasma membrane. In the absence of Mn^{2+}, there was no obvious MnDDC signal (TAMRA, red) on cells surface (Figure 4B, lane 1). Upon the addition of exogenous Mn^{2+}, significant red fluorescence signals were observed on the surface of CEM cells, while no obvious red fluorescence signals were detected in the control groups (Figure 4B). Owing to the inherently high structural stability and low background fluorescence of MB, this MnDDC-based sensor allows direct monitoring of the fluorescence signal by a confocal microscopy without extra wash steps. The red fluorescence was perfectly overlapped with the fluorescence of EGFP, suggesting the coupling of the DNA fragment on the cell surface. In order to avoid the influence caused by protein expression level, the average ratio (I_{red}/I_{green}) signal was used to quantitatively evaluate the results. The semi-quantitative results quantified by ImageJ revealed that the average ratio increased 7.0-fold in the presence of Mn^{2+} compared to that in the absence of Mn^{2+} (Figure 4D). Furthermore, real-time imaging was performed to analyze the dynamic process of the reaction, and the average ratio rapidly increased within 0.5 min and reached saturation in 2 min (Figure 4C and 4E). Since the fluorescence intensity of GFP remained stable (Figure S8), the quick response suggested that the reaction on cell surface is almost the same as that for MnDDC in buffer solution. Collectively, based on the intrinsic clickable characteristics, MnDDC, with robust "one-pot" and fast procedure and good selectivity, opens a new window for wash-free and rapid Mn^{2+} detection on living cell surface, thus exhibiting great potential for subcellular localization imaging.

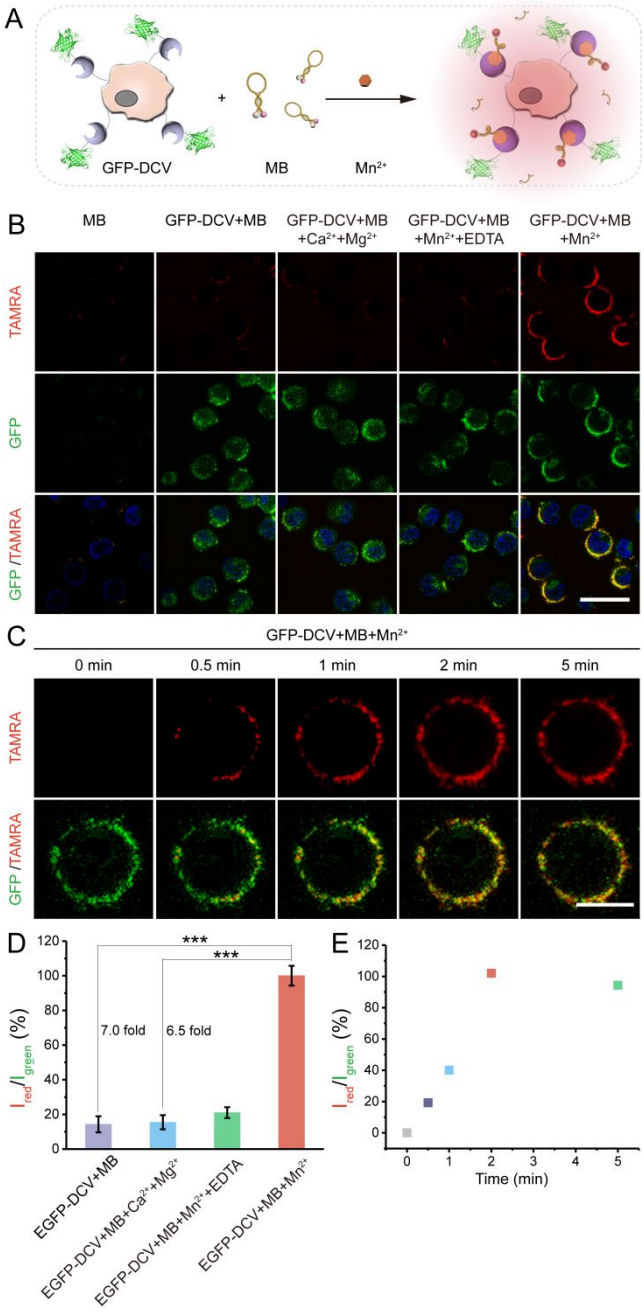

Figure 4. (A) Schematic of wash-free Mn^{2+} imaging on CEM cell surface. (B) Fluorescence images of Mn^{2+} on CEM cell surface at 20 ℃, where GFP-DCV is displayed on cell surface with the help of pDisplay vector. The mixture was incubated at 20 ℃ for 5 min. Scale bar is 30 μm. (C) Dynamic fluorescence images on a single CEM cell surface. Scale bar is 10 μm. (D) Semi-quantitative results of the average ratio (I_{red}/I_{green}) signal in Figure 3B. Data points represent mean ± SD (n = 10). ***$p < 0.001$. (E) Semi-quantitative results of ratio (I_{red}/I_{green}) signal in Figure 3C. Red: TAMRA, green: GFP, blue: Hoechst 33342. GFP-DCV is endogenous expressed. [MB] = 100 nM, [Mn^{2+}] = 500 μM, [Mg^{2+}] = 250 μM, [Ca^{2+}] = 250 μM, [EDTA] = 500 μM.

Cellular Responses of Neural Cells Towards the Disordered Homeostasis of Mn^{2+}. Although Mn is an essential heavy metal, chronic overexposure and disordered homeostasis of Mn^{2+} are closely related to mental disturbances, movement disorders and other brain-related toxicities.[21, 22, 30] Various biology researches focused on neurotoxic effects of Mn^{2+}, while additional studies are still in highly needed for visual monitoring of the

correlation between Mn homeostasis alteration and the corresponding cellular downstream response in neural cells. Encouraged by the excellent preformance of the MnDCC-based sensor in living cell imaging of Mn^{2+}, we validated the feasibility of the proposed sensor for Mn^{2+} imaging during exploration of the associated cellular responses.

The important pathogenic role of Mn^{2+} has been well illustrated in previous research as its ability of increasing oxidative stress and subsequently inducing neuronal death.[21, 35] To verify the relationship between Mn^{2+} fluctuation and reactive oxygen species (ROS) generation, the Mn^{2+} level was visualized by the red fluorescence of the MnDDC-based sensor, and the corresponding ROS level in cells was imaged by the green fluorescence of the commercial ROS probe 2′,7′-dichlorofluorescein (DCF, Figure 5A).[36, 37] In this work, SHSY5Y cell, a commonly used cell line in neural research,[38, 39] was chosen as a model, and transfected with DCV and/or MB, and incubated with different metal ions. As shown in Figure 5B, 5C and Figure S9, the red fluorescence in cytoplasm of the Mn^{2+}-treated cells increased 7.3-fold compared to that in untreated control cells, indicating the intracellular accumulation of Mn^{2+}. Meanwhile, the distinct green fluorescence signal of ROS emerged in the Mn^{2+}-treated cells, which is 5.5-fold as high as that in normal SHSY5Y cells (Figure S9). While in the control cell groups, neither the red fluorescence of the Mn^{2+} accumulation nor the intensive green fluorescence of ROS were observed in the cytoplasm. Additionally, the results of CCK8 assay revealed that the cell viability of SHSY5Y cells decreased 50.2% after the incubation of Mn^{2+}, while the MnDDC-based sensor showed no apparent cytotoxicity, suggesting the neurotoxicity of Mn^{2+} (Figure S10). Therefore, these results indicated that Mn^{2+} uptake and ROS generation can be detected at the same time by our method and the ROS probe, respectively, and the elevated intracellular Mn^{2+} level in nerve cells could induce large amount of endogenous ROS, leading to the cell deactivation or death through mitochondrial damage.[35, 40]

Dopaminergic dysfunction has been proved to be a pathogenic effect of elevated Mn^{2+} level in diseases such as Manganism and Parkinson's disease.[21, 22, 41] Tyrosine hydroxylase (TH) is the rate-limiting enzyme in dopamine synthesis in nervous system.[42] Extracellular Mn^{2+} is closely related with Mn^{2+} uptake and plays a vital role in Mn biology process.[43] Hence, the tyrosine hydroxylase (TH) level was chosen as a target to verify the cellular response towards extracellular microenvironmental Mn^{2+} homeostasis alteration (Figure 5D). Firstly, DCV was displayed on the extracellular plasma membrane of SHSY5Y cells by the pDisplay system, and the practicability of the MnDDC-based sensor for selective sensing extracellular Mn^{2+} was proved firstly (Figure S11). In the following, extracellular Mn^{2+} level was monitored by the MnDDC-based sensor (Figure 5E), and the corresponding TH expression level in SHSY5Y cells was analyzed by immunofluorescence (IF) (Figure 5F) and western blot (WB) (Figure 5G), respectively. When the cells were incubated with 100 μM Mn^{2+}, the red fluorescence signal of the MnDDC-based sensor increased 5-fold, and the TH level quantified by IF decreased 50.0%, which was further validated by WB. A higher concentration of extracellular Mn^{2+} (250 μM) caused a further increased red fluorescence signal (20-fold), along with a further decline of 75.0% in TH level. Moreover, a similar Mn^{2+}-dependent down-regulation of TH level was also observed in human glioma cells (U251, Figure S12). Therefore, taking the advantage of the MnDDC-based sensor, visualization of both extracellular and cytoplasmic Mn^{2+} levels have been achieved, based on which relevance between the elevated Mn^{2+} level with the neuropathological consequences, including ROS generation and decreased TH expression, has been demonstrated.

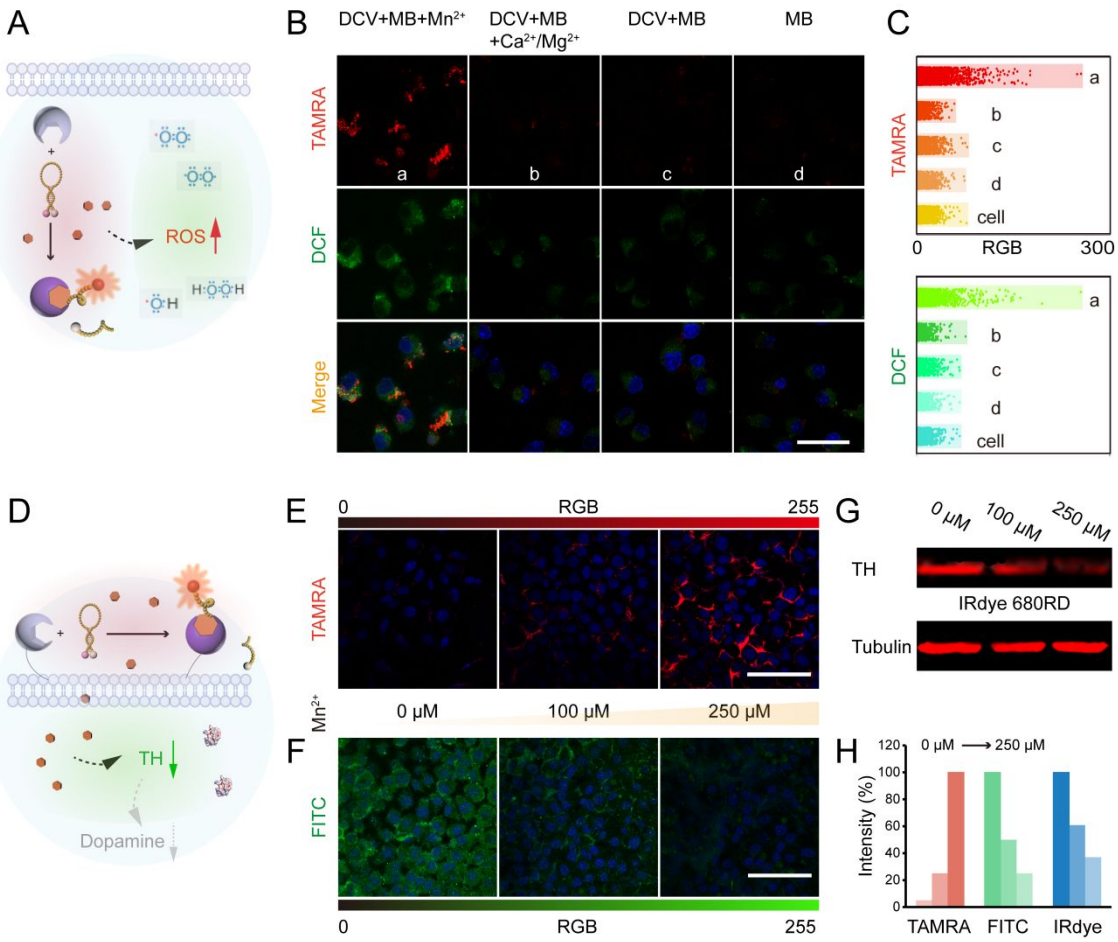

Figure 5. Cellular responses of the neural cells towards disordered homeostasis of Mn^{2+}. (A) Schematic of the cytoplasmic Mn^{2+} sensing and ROS generation in living cells. (B) CLSM images of Mn^{2+} detection from TAMRA signal of MnDDC, and ROS assay by DCF in SHSY5Y cell. Red: TAMRA, green: DCF, blue: Hoechst 33342. Scale bar is 25 μm. [DCV] = 1 μM, [MB] = 100 nM, [Mn^{2+}] = 500 μM, [Mg^{2+}] = 250 μM, [Ca^{2+}] = 250 μM. DCV and MB were transfected into cells by Lipofectamine 3000. (C) Red and green fluorescence signal distributions of each pixel in Figure 5B. (D) Schematic of the extracellular Mn^{2+} monitoring and the corresponding cellular response (TH expression) towards the disordered homeostasis of Mn^{2+}. (E) CLSM images of the extracellular Mn^{2+} by the MnDDC-based sensor. Scale bar is 100 μm. [MB] = 100 nM, [Mn^{2+}] = 0-250 μM. DCV is displayed on cell surface with the help of pDisplay vector. (F) IF imaging of TH levels in cells at different concentrations of extracellular Mn^{2+} (0-250 μM). Green: FITC, blue: DAPI. Scale bar is 100 μm. (G) TH levels in the present of different concentrations of extracellular Mn^{2+} quantified by WB. (H) Normalized results of the MnDDC-based sensor (Figure 5E), IF (Figure 5F) and WB (Figure 5G) signals. Cells were incubated with Mn^{2+} for 12 h at 37 ℃.

CONCLUSIONS

In summary, a Mn^{2+}-activated DCV-DNA conjunction (MnDDC) was characterized as a click-type reaction. On the basis of the high specificity of the reaction towards Mn^{2+}, an MnDDC-based assay was developed for rapid and sensitive sensing of Mn^{2+}. The click characteristics enable this assay for Mn^{2+} detection not only in serum and food samples, but also in living cells without additional wash steps. Moreover, benefiting from the protein nature of DCV, it was deployed as a subcellular targeting sensor on cell surface for Mn^{2+} monitoring in the extracellular microenvironment. Using this sensor as a tool for Mn^{2+} visualizing in living neural cells, the cellular responses towards the disordered homeostasis of Mn^{2+} both in extracellular and intracellular

microenvironment have been validated. Furthermore, our work demonstrated that the click-type MnDDC is suitable for site-specific covalent protein-DNA linkage in complex biological environments, which sheds light on potential applications of natural click type reactions for bioanalysis and biological research.

AUTHOR INFORMATION

Corresponding Author

E-mail: huangyan.hnu@gmail.com; niezhou.hnu@gmail.com.

Author Contributions

Shanfang Hu and Jinghui Zhang contributed equally to this work.

Notes

The authors declare no competing financial interest.

ACKNOWLEDGMENT

The authors are grateful to the National Natural Science Foundation of China (Nos. 21675044, 21725503, 21575038), the Young Top-notch Talent for Ten Thousand Talent Program, and the Hunan Provincial Natural Science Foundation of China No. 2017JJ1009.

Supporting Information Available

Supplementary Information including Tables S1-S4 and Figure S1-S12 are available free of charge via the Internet at http://pubs.acs.org.

REFERENCES

(1) Kolb, H. C.; Finn, M. G.; Sharpless, K. B. Click chemistry: diverse chemical function from a few good reactions. *Angew. Chem. Int. Ed*. **2001**, *40*, 2004-2021.

(2) Thirumurugan, P.; Matosiuk, D.; Jozwiak, K. Click chemistry for drug development and diverse chemical-biology applications. *Chem. Rev.* **2013**, *113*, 4905-4979.

(3) Nandivada, H.; Jiang, X.; Lahann, J. Click chemistry: versatility and control in the hands of materials scientists. *Adv. Mater.* **2007**, *19*, 2197-2208.

(4) Saal, Kim-A.; Richter, F.; Rehling, P.; Rizzoli, S. O. Combined Use of Unnatural Amino Acids Enables Dual-Color Super-Resolution Imaging of Proteins via Click Chemistry. *ACS Nano* **2018**, *12*, 12247–12254.

(5) Yang, M.; Li, J.; Chen, P. R. Transition metal-mediated bioorthogonal protein chemistry in living cells. *Chem. Soc. Rev.* **2014**, *43*, 6511-6526. (b) Lauer, M. H.; Vranken, C.; Deen, J.; Frederickx, W.; Vanderlinden, W.; Wand, N.; Leen, V.; Gehlen, M. H.; Hofkensa, J.; Neely, R. K. Methyltransferase-directed covalent coupling of fluorophores to DNA. *Chem. Sci.* **2017**, *8*, 3804-3811.

(6) Lauer, M. H.; Vranken, C.; Deen, J.; Frederickx, W.; Vanderlinden, W.; Wand, N.; Leen, V.; Gehlen, M. H.; Hofkensa, J.; Neely, R. K. Methyltransferase-directed covalent coupling of fluorophores to DNA. *Chem. Sci.* **2017**, *8*, 3804-3811.

(7) El-Sagheer, A. H.; Brown, T. Click nucleic acid ligation: applications in biology and nanotechnology. *Acc. Chem. Res.* **2012**, *45*, 1258-1267.

(8) Bisseret, P.; Abdelkafi, H.; Blanchard, N. Aryl transition metal chemical warheads for protein bioconjugation. *Chem. Sci.* **2018**, *9*, 5132-5144.

(9) Wolfbeis, O. S. The click reaction in the luminescent probing of metal ions, and its implications on biolabeling techniques. *Angew. Chem. Int. Ed.* **2007**, *46*, 2980-2982.

(10) Manderville, R. A.; Wetmore, S. D. C-Linked 8-aryl guanine nucleobase adducts: biological outcomes and utility as fluorescent probes. *Chem. Sci.* **2016**, *7*, 3482–3493.

(11) Trads, J. B.; Tørring, T.; Gothelf, K. V. Site-selective conjugation of native proteins with DNA. *Acc. Chem. Res.* **2017**, *50*, 1367-1374.

(12) Chen, T. Y.; Cheng, Y. S.; Huang, P. S.; Chen, P. Facilitated unbinding via multivalency-enabled ternary complexes: new paradigm for protein–DNA interactions. *Acc. Chem. Res.* **2018**, *51*, 860–868.

(13) Praetorius, F.; Dietz, H. Self-assembly of genetically encoded DNA-protein hybrid nanoscale shapes. *Science* **2017**, *355*, eaam5488.

(14) Siggers, T.; Gordân, R. Protein–DNA binding: complexities and multi-protein codes. *Nucleic Acids Res.* **2014**, *42*, 2099-2111.

(15) Chandler, M.; Cruz, F. de la; Dyda, F.; Hickman, A. B.; Moncalian, G.; Ton-Hoang, B. Breaking and joining single-stranded DNA: the HUH endonuclease superfamily. *Nat. Rev. Microbiol.* **2013**, *11*, 525-538.

(16) Steinfeldt, T.; Finsterbusch, T.; Mankertz, A. Demonstration of nicking/joining activity at the origin of DNA replication associated with the rep and rep′ proteins of porcine circovirus type 1. *J. Virol.* **2006**, *80*, 6225-6234.

(17) Lovendahl, K. N.; Hayward, A. N.; Gordon, W. R. Sequence-directed covalent protein–DNA linkages in a single step using HUH-tags. *J. Am. Chem. Soc.* **2017**, *139*, 7030-7035.

(18) Hattermann, K.; Schmitt, C.; Soike, D.; Mankertz, A. Cloning and sequencing of Duck circovirus (DuCV). *Arch. Virol.* **2003**, *148*, 2471–2480.

(19) Reddi, A. R.; Jensen, L. T.; Culotta, V. C. Manganese Homeostasis in Saccharomyces cerevisiae. *Chem. Rev.* **2009**, *109*, 4722-4732.

(20) Dambach, M.; Sandoval, M.; Updegrove, T. B.; Anantharaman, V.; Aravind, L.; Waters, L. S.; Storz, G. The ubiquitous yybP-ykoY riboswitch is a manganese-responsive regulatory element. *Mol. Cell* **2015**, *57*, 1099-1109.

(21) Horning, K. J.; Caito, S. W.; Tipps, K. G.; Bowman, A. B.; Aschner, M. Manganese is essential for neuronal health. *Annu. Rev. Nutr.* **2015**, *35*, 71-108.

(22) Guilarte, T. R. Manganese and Parkinson's disease: a critical review and new findings. *Environ. Health Perspect.* **2010**, *118*, 1071-1080.

(23) Carter, K. P.; Young, A. M.; Palmer, A. E. Fluorescent sensors for measuring metal ions in living systems. *Chem. Rev.* **2014**, *114*, 4564-4601.

(24) Hu, S.; Chen, X.; Lei, C.; Tang, R.; Kang, W.; Deng, H.; Huang, Y.; Nie, Z.; Yao, S. Charge designable and tunable GFP as a target pH-responsive carrier for intracellular functional protein delivery and tracing. *Chem. Commun*. **2018**, *54*, 7806-7809.

(25) Zhou, W.; Saran, R.; Liu ,J. Metal sensing by DNA. *Chem. Rev.* **2017**, *117*, 8272-8325.

(26) Vega-Rocha, S.; Byeon, I. J. L.; Gronenborn, B.; Gronenborn, A. M.; Campos-Olivas, R. Solution structure, divalent metal and DNA binding of the endonuclease domain from the replication initiation protein from porcine circovirus 2. *J. Mol. Biol.* **2007**, *367*, 473-487.

(27) Xianyu, Y.; Wang Z.; Jiang X. A Plasmonic Nanosensor for Immunoassay via Enzyme-Triggered Click Chemistry. *Acs Nano* **2014**, *8*, 12741-12747.

(28) Zeng, Y.; Ren, J. Q.; Shen, A. G.; Hu, J. M. Splicing Nanoparticles-Based "Click" SERS Could Aid Multiplex Liquid Biopsy and Accurate Cellular Imaging. *J. Am. Chem. Soc.* **2018**, *140*, 10649-10652.

(29) Lechpammer, M.; Clegg, M. S.; Muzar, Z.; Huebner, P. A.; Jin, L. W.; Gospe, S. M. Pathology of inherited manganese transporter deficiency. *Ann. Neurol.* **2014**, *75*, 608-612.

(30) Peres, T. V.; Schettinger, M. R. C.; Chen, P.; Carvalho F,.; Avila, D. S.; Bowman, A. B.; Aschner, M. Manganese-induced neurotoxicity: a review of its behavioral consequences and neuroprotective strategies. *BMC Pharmacol Toxicol* **2016**, *17*, 57-77.

(31) Gruppi, F.; Liang, J.; Bartelle, B. B.; Royzen, M.; Turnbull, D. H.; Canary, J. W. Supramolecular metal displacement allows on-fluorescence analysis of manganese (II) in living cells. *Chem. Commun.* **2012**, *48*, 10778-10780.

(32) Dai, Z.; Khosla, N.; Canary, J. W. Visible colour displacement sensing system for manganese (II). *Supramol. Chem.* **2009**, *21*, 296-300.

(33) Hozumi, I.; Hasegawa, T.; Honda, A.; Ozawa, K.; Hayashi, Y.; Hashimoto, K.; Yamada, M.; Koumura, A.; Sakurai, T.; Kimura, A.; Tanaka, Y.; Satoh, M.; Inuzuka, T. Patterns of levels of biological metals in CSF differ among neurodegenerative diseases. *J. Neurol. Sci.* **2011***, 303*, 95-99.

(34) Choi, Y. A.; Keem, J. O.; Kim, C. Y.; Yoon, H. R.; Heo, W. D.; Chung, B.H.; Jung, Y. A novel copper-chelating strategy for fluorescent proteins to image dynamic copper fluctuations on live cell surfaces. *Chem. Sci.* **2015**, *6*, 1301-1307.

(35) Stuntz, E.; Gong, Y.; Sood, D.; Liaudanskaya, V.; Pouli, D.; Quinn, K. P.; Alonzo, C.; Liu, Z.; Kaplan, D. L.; Georgakoudi, I. Endogenous two-photon excited fluorescence imaging characterizes neuron and astrocyte metabolic responses to manganese toxicity. *Sci. Rep.* **2017**, *7*, 1041-1055.

(36) He, T.; Ren, C.; Luo, Y.; Wang, Q.; Li, J.; Lin, X.; Ye, C.; Hu, W.; Zhang, J. Water-soluble chiral tetrazine derivatives: towards the application of circularly polarized luminescence from upper-excited states to photodynamic therapy. *Chem. Sci.* **2019**, *10*, 4163-4168.

(37) Dong, S.; Xu, J.; Jia, T.; Xu, M.; Zhong, C.; Yang, G.; Li, J.; Yang, D.; He, F.; Gai, S.; Yang, P.; Lin, J. Upconversion-mediated ZnFe2O4 nanoplatform for NIR-enhanced chemodynamic and photodynamic therapy. *Chem. Sci.* **2019**, *10*, 4259-4271.

(38) Xicoy, H.; Wieringa, B.; Martens, G. J.M. The SH-SY5Y cell line in Parkinson's disease research: a systematic review. *Mol. Neurodegener.* **2017**, *12*, 10-21.

(39) Sartori-Rupp, A.; Cervantes, D. C.; Pepe, A.; Gousset, K.; Delage, E.; Corroyer-Dulmont, S.; Schmitt, C.; Krijnse-Locker, J.; Zurzolo, C. Correlative cryo-electron microscopy reveals the structure of TNTs in neuronal cells. *Nat. Commun.* **2019**, *10*, 342-357.

(40) Roth, J. A. Are there common biochemical and molecular mechanisms controlling manganism and parkisonism. *Neuromol. Med.* **2009**, *11*,281-296.

(41) Chen, W.; Huang, Q.; Ma, S.; Li, M. Progress in Dopaminergic Cell Replacement and Regenerative Strategies for Parkinson's Disease. *ACS Chem. Neurosci.* **2019**, *10*, 839-851.

(42) Logan, R. W.; McClung, C. A. Rhythms of life: circadian disruption and brain disorders across the lifespan. *Nat. Rev. Neurosci.* **2019**, *20*, 49-65.

(43) Chen, Y.; Shen, Y.; Wang, W. Mn^{2+} modulates the expression of cellulase genes in Trichoderma reesei Rut-C30 via calcium signalling. *Biotechnol. Biofuels.* **2018**, *11*, 54-72.

Table of Contents

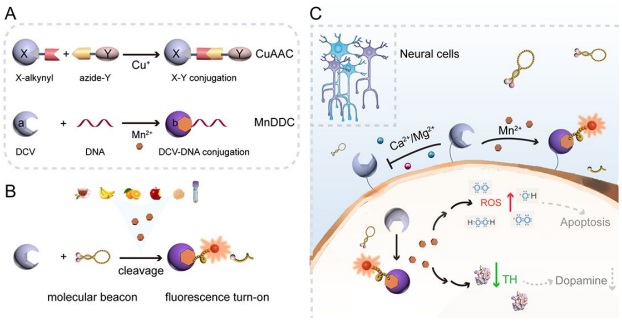

A click-type protein-DNA conjugation for Mn^{2+} imaging in living cells.